

Continual Vision-based Reinforcement Learning with Group Symmetries

Anonymous Author(s)

Affiliation

Address

email

1 **Abstract:** Continual reinforcement learning aims to sequentially learn a variety
2 of tasks, retaining the ability to perform previously encountered tasks while si-
3 multaneously developing new policies for novel tasks. However, current contin-
4 ual RL approaches overlook the fact that certain tasks are identical under basic
5 group operations like rotations or translations, especially with visual inputs. They
6 may unnecessarily learn and maintain a new policy for each similar task, lead-
7 ing to poor sample efficiency and weak generalization capability. To address this,
8 we introduce a unique **C**ontinual **V**ision-based **R**einforcement Learning method
9 that recognizes Group **S**ymmetries, called COVERS, cultivating a policy for each
10 group of equivalent tasks rather than an individual task. COVERS employs a
11 proximal policy gradient-based (PPO-based) algorithm to train each policy, which
12 contains an equivariant feature extractor and takes inputs with different modalities,
13 including image observations and robot proprioceptive states. It also utilizes an
14 unsupervised task clustering mechanism that relies on 1-Wasserstein distance on
15 the extracted invariant features. We evaluate COVERS on a sequence of table-top
16 manipulation tasks in simulation and on a real robot platform. Our results show
17 that COVERS accurately assigns tasks to their respective groups and significantly
18 outperforms baselines by generalizing to unseen but equivariant tasks in seen task
19 groups. Demos are available on our project page¹.

20 **Keywords:** Continual Learning, Symmetry, Manipulation

21 1 INTRODUCTION

22 Quick adaptation to unseen tasks has been a key objective in the field of reinforcement learning
23 (RL) [1, 2, 3]. RL algorithms are usually trained in simulated environments and then deployed
24 in the real world. However, pre-trained RL agents are likely to encounter new tasks during their
25 deployment due to the nonstationarity of the environment. Blindly reusing policies obtained during
26 training can result in substantial performance drops and even catastrophic failures [4, 5].

27 Continual RL (CRL), also referred to as lifelong RL, addresses this issue by sequentially learning
28 a series of tasks. It achieves this by generating task-specific policies for the current task, while si-
29 multaneously preserving the ability to solve previously encountered tasks [3, 6, 7, 8, 9]. Existing
30 CRL works that rely on the task delineations to handle non-stationary initial states, dynamics or re-
31 ward functions can greatly boost task performance, particularly when significant task changes occur
32 [7]. However, in realistic task-agnostic settings, these delineations are unknown a priori and have to
33 be identified by the agents. In this work, we explore *how to define and detect task delineations to*
34 *enhance robots’ learning capabilities in task-agnostic CRL.*

35 Our key insight is that robotic control tasks typically preserve certain desirable structures, such as
36 *group symmetries*. Existing CRL approaches typically delineate task boundaries based on statistical

¹Project Page: <https://sites.google.com/view/rl-covers/>.

37 measures, such as maximum a posteriori estimates and likelihoods [7, 8]. However, these mea-
 38 sures overlook the geometric information inherent in task representations, which naturally emerge
 39 in robotic control tasks, as demonstrated in Figure 1. Consider the drawer-closing example: con-
 40 ventional CRL works using image inputs would treat each mirrored configuration as a new task and
 41 learn the task from scratch. Yet, we, as humans, understand that the mirrored task configuration can
 42 be easily resolved by correspondingly reflecting the actions. Learning the mirrored task from scratch
 43 hampers positive task interference and limits the agent’s adaptivity. To address this issue, our goal
 44 is to exploit the geometric similarity among tasks in the task-agnostic CRL setting to facilitate rapid
 45 adaptation to unseen but geometrically equivalent tasks.

46 In this work, we propose COVERS, a task-
 47 agnostic vision-based CRL algorithm with strong
 48 sample efficiency and generalization capability
 49 by encoding group symmetries in the state and ac-
 50 tion spaces. We define a *task group* as the set that
 51 contains equivalent tasks under the same group
 52 operation, such as rotations and reflections. We
 53 state our main contributions as follows:

- 54 1. COVERS grows a PPO-based [10] policy
 55 with an equivariant feature extrac-
 56 tor for each task group, instead of a single
 57 task, to solve unseen tasks in seen
 58 groups in a zero-shot manner.
- 59 2. COVERS utilizes a novel unsupervised
 60 task grouping mechanism, which au-
 61 tomatically detects group boundaries
 62 based on 1-Wasserstein distance in the
 63 invariant feature space.
- 64 3. In non-stationary table-top manipulation
 65 environments, COVERS performs better than baselines in terms of average rewards and
 66 success rates. Moreover, we show that (a) the group symmetric information from the equiv-
 67 ariant feature extractor promotes the adaptivity by maximizing the positive interference
 68 within each group, and (b) the task grouping mechanism recovers the ground truth group
 69 indexes, which helps minimize the negative interference among different groups.

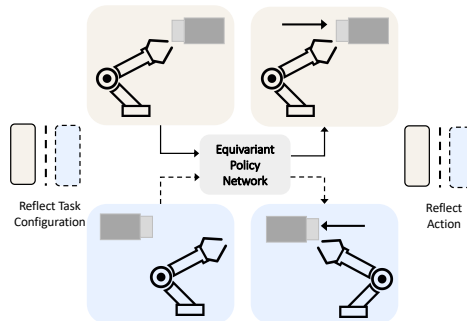


Figure 1: This example illustrates how group symmetry enhances adaptability. The robot is instructed to close drawers situated in two distinct locations with top-down images as inputs. Considering the symmetry of the drawers’ locations around the robot’s position, the optimal control policies are equivalent but mirrored.

70 2 Related Work

71 **Task-Agnostic CRL.** CRL has been a long-standing problem that aims to train RL agents adaptable
 72 to non-stationary environments with evolving world models [11, 12, 13, 14, 15, 5, 16, 17, 18, 19]. In
 73 task-agnostic CRL where task identifications are unrevealed, existing methods have addressed the
 74 problem through a range of techniques. These include hierarchical task modeling with stochastic
 75 processes [7, 8], meta-learning [3, 20], online system identification [21], learning a representation
 76 from experience [9, 22], and experience replay [14, 23]. Considering that in realistic situations, the
 77 new task may not belong to the same task distribution as past tasks, we develop an ensemble model of
 78 policy networks capable of handling diverse unseen tasks, rather than relying on a single network to
 79 model dynamics or latent representations. Moreover, prior work often depends on data distribution-
 80 wise similarity or distances between latent variables, implicitly modeling task relationships. In
 81 contrast, we aim to introduce beneficial inductive bias explicitly by developing policy networks
 82 with equivariant feature extractors to capture the geometric structures of tasks.

83 **Symmetries in RL.** There has been a surge of interest in modeling symmetries in components of
 84 Markov Decision Processes (MDPs) to improve generalization and efficiency [24, 25, 26, 27, 28, 29,
 85 30, 31, 32, 33, 34, 35]. MDP homomorphic network [26] preserves equivariant under symmetries in
 86 the state-action spaces of an MDP by imposing an equivariance constraint on the policy and value

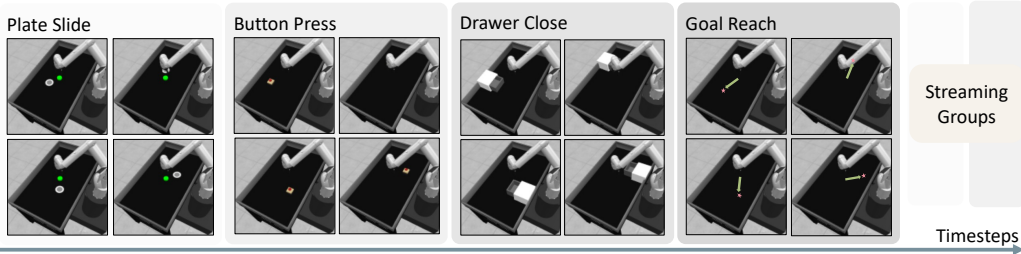


Figure 2: The continual learning environment setup involves four task groups, including Plate Slide, Button Press, Drawer Close, and Goal Reach. Groups streamingly come in.

87 network. As a result, it reduces the RL agent’s solution space and increases sample efficiency. This
 88 single-agent MDP homomorphic network is then extended to the multi-agent domain by factorizing
 89 global symmetries into local symmetries [27]. SO(2)-Equivariant RL [28] extends the discrete sym-
 90 metry group to the group of continuous planar rotations, SO(2), to boost the performance in robotic
 91 manipulation tasks. In contrast, we seek to exploit the symmetric properties to improve the general-
 92 ization capability of task-agnostic CRL algorithms and handle inputs with multiple modalities.

93 3 Preliminary

94 **Markov decision process.** We consider a Markov decision process (MDP) as a 5-tuple
 95 $(\mathcal{S}, \mathcal{A}, T, R, \gamma)$, where \mathcal{S} and \mathcal{A} are the state and action space, respectively. $T : \mathcal{S} \times \mathcal{A} \rightarrow \Delta(\mathcal{S})$
 96 is the transition function, $R : \mathcal{S} \times \mathcal{A} \rightarrow \mathbb{R}$ is the reward function, and γ is the discount factor. We
 97 aim to find an optimal policy $\pi_\theta : \mathcal{S} \rightarrow \mathcal{A}$ parameterized by θ that maximizes the expected return
 98 $\mathbb{E}_{\tau \sim \pi_\theta} \left[\sum_{t=0}^{H-1} \gamma^t r(s_t, a_t) \right]$, where H is the episode length.

99 **Invariance and equivariance.** Let G be a mathematical group. $f : \mathcal{X} \rightarrow \mathcal{Y}$ is a mapping function.
 100 For a transformation $L_g : \mathcal{X} \rightarrow \mathcal{X}$ that satisfies $f(x) = f(L_g[x]), \forall g \in G, x \in \mathcal{X}$, we say f is
 101 invariant to L_g . Equivariance is closely related to invariance. If we can find another transformation
 102 $K_g : \mathcal{Y} \rightarrow \mathcal{Y}$ that fulfills $K_g[f(x)] = f(L_g[x]), \forall g \in G, x \in \mathcal{X}$ then we say f is equivariant to
 103 transformation L_g . It’s worth noting that invariance is a special case of equivariance.

104 **MDP with group symmetries.** In MDPs with symmetries [24, 25, 26], we can identify at least one
 105 mathematical group G of a transformation $L_g : \mathcal{S} \rightarrow \mathcal{S}$ and a state-dependent action transformation
 106 $K_g^s : \mathcal{A} \rightarrow \mathcal{A}$, such that $R(s, a) = R(L_g[s], K_g^s[a]), T(s, a, s') = T(L_g[s], K_g^s[a], L_g[s'])$ hold
 107 for all $g \in G, s, s' \in \mathcal{S}, a \in \mathcal{A}$.

108 **Equivariant convolutional layer.** Let G be a Euclidean group, with the special orthogonal group
 109 and reflection group as subgroups. We use the equivariant convolutional layer developed by Weiler
 110 and Cesa [36], where each layer consists of G -steerable kernels $k : \mathbb{R}^2 \rightarrow \mathbb{R}^{c_{\text{out}} \times c_{\text{in}}}$ that satisfies
 111 $k(gx) = \rho_{\text{out}}(g)k(x)\rho_{\text{in}}(g^{-1}), \forall g \in G, x \in \mathbb{R}^2$. ρ_{in} and ρ_{out} are the types of input vector field
 112 $f_{\text{in}} : \mathbb{R}^2 \rightarrow \mathbb{R}^{c_{\text{in}}}$ and output vector field $f_{\text{out}} : \mathbb{R}^2 \rightarrow \mathbb{R}^{c_{\text{out}}}$, respectively.

113 **Equivariant MLP.** An equivariant multi-layer perceptron (MLP) consists of both equivariant linear
 114 layers and equivariant nonlinearities. An equivariant linear layer is a linear function W that maps
 115 from one vector space V_{in} with type ρ_{in} to another vector space with type ρ_{out} for a given group G .
 116 Formally $\forall x \in V_{\text{in}}, \forall g \in G : \rho_{\text{out}}(g)Wx = W\rho_{\text{in}}(g)x$. Here we use the numerical method proposed
 117 by Finzi et al. [37] to parameterize MLPs that are equivariant to arbitrary groups.

118 4 Methodology

119 4.1 Problem Formulation

120 We focus on continual learning in table-top manipulation environments, where various tasks are
 121 sequentially presented. We hypothesize that the streaming tasks can be partitioned into task groups,
 122 each containing tasks that share symmetry with one another. We adopt a realistic setting where a
 123 new task group may emerge at each episode, the total number of distinct groups remains unknown

Algorithm 1 COVERS: Continual Vision-based RL with Group Symmetries

Input: Threshold d_ϵ , initial frame number k , update interval N_u , rollout step size N_s

Output: collection of policies Π

Initialization: Current policy π_{cur} initialized as a random policy with a policy data buffer $\mathcal{B} \leftarrow \emptyset$, policy collection $\Pi \leftarrow \{(\pi_{cur}, \mathcal{B})\}$, number of episodes $n \leftarrow 0$, online rollout buffer $\mathcal{D} \leftarrow \emptyset$

```
1: while task not finish do
2:    $n \leftarrow n + 1$ 
3:   if  $n \% N_u = 0$  then
4:     Rollout buffer  $\mathcal{O} \leftarrow \emptyset$  ▷ Unsupervised Policy Assignment
5:     Rollout  $N_s$  steps with  $\pi_{cur}$  and get trajectories  $\tau = \{(s_0, a_0, \dots, s_H, a_H)\}$ 
6:     Append the first  $k$  frames of each episode to rollout buffer  $\mathcal{O} \leftarrow \{(s_0, \dots, s_{k-1})\}$ 
7:     Append the whole episode trajectories  $\tau$  to the online rollout buffer  $\mathcal{D}$ 
8:     Calculate the 1-Wasserstein distances  $d_i^W(\mathcal{O}, \mathcal{B}_i), \forall \{\pi_i, \mathcal{B}_i\} \in \Pi$  (Equation 2)
9:     Get the minimum distance  $d_j^W$  where  $j = \arg \min_i d_i^W(\mathcal{O}, \mathcal{B}_i)$ 
10:    if  $d_j > d_\epsilon$  then
11:      Initialize a new random policy  $\pi$  as well as its policy data buffer  $\mathcal{B} \leftarrow \mathcal{O}$ 
12:       $\pi_{cur} \leftarrow \pi, \Pi \leftarrow \Pi \cup \{(\pi, \mathcal{B})\}$ 
13:    else
14:      Assign the existing policy and buffer with  $\pi_{cur} \leftarrow \pi_j, \mathcal{B}_j \leftarrow \mathcal{B}_j \cup \mathcal{O}$ 
15:      Update  $\pi_{cur}$  based on online rollout buffer  $\mathcal{D}$  (Equation 1) ▷ Equivariant Policy Update
16:       $\mathcal{D} \leftarrow \emptyset$ 
17:    else
18:      Sample an episode and append to online rollout buffer  $\mathcal{D}$ 
```

124 and the group may arrive in random orders. The primary objective is to devise an online learning
125 algorithm capable of achieving high performance across all tasks with strong data efficiency. We
126 visualize our CRL setting with table-top manipulation environments in Figure 2.

127 4.2 Algorithm

128 We present the pseudocode for COVERS, a task-agnostic continual RL method with group sym-
129 metries, in Algorithm 1. COVERS maintains a collection $\Pi = \{(\pi, \mathcal{B})\}$, each element of which
130 comprising a pair of policy π and its respective data buffer \mathcal{B} . Each policy π independently manages
131 one group of tasks, with \mathcal{B} storing the initial frames of the group it oversees. At fixed time intervals,
132 COVERS collects N_s steps in parallel under the current policy π_{cur} and stores the first k frames
133 from each episode in the rollout buffer \mathcal{O} . Based on \mathcal{O} , the algorithm then either (a) creates a new
134 policy for an unseen group and adds it to the collection Π , or (b) recalls an existing policy from
135 the collection Π if the group has been previously encountered. It is worth noting that we assign
136 policies based on initial frames of each episode rather than the full episode rollout. This is because
137 frames corresponding to later timesteps are heavily influenced by the behavior policy and could eas-
138 ily lead to unstable policy assignments. Only maintaining a subset of the rollout trajectories also
139 helps alleviate memory usage.

140 After the policy assignment, the selected policy π_{cur} with parameters θ is updated based on an online
141 rollout buffer \mathcal{D} and Proximal Policy gradient (PPO) method [10] with loss in Equation 1. \hat{A}_t is the
142 estimated advantage, $\rho_t = \pi_\theta(a_t|s_t)/\pi_{\theta_{old}}(a_t|s_t)$ is the importance ratio and ϵ is the clip range.

$$\mathcal{L}_{CLIP} = \mathbb{E}_{\tau \sim \mathcal{D}} \left[\sum_{t=1}^H \min[\rho_t(\theta)\hat{A}_t, \text{clip}(\rho_t(\theta), 1 - \epsilon, 1 + \epsilon)\hat{A}_t] \right]. \quad (1)$$

143 4.3 Policy Network Architecture

144 COVERS utilizes an equivariant policy network that comprises a policy network for predicting ac-
145 tions, a value network approximating values, and an equivariant feature extractor taking multiple
146 modalities. We show the policy architecture in Figure 3 and additional details in Figure 10.

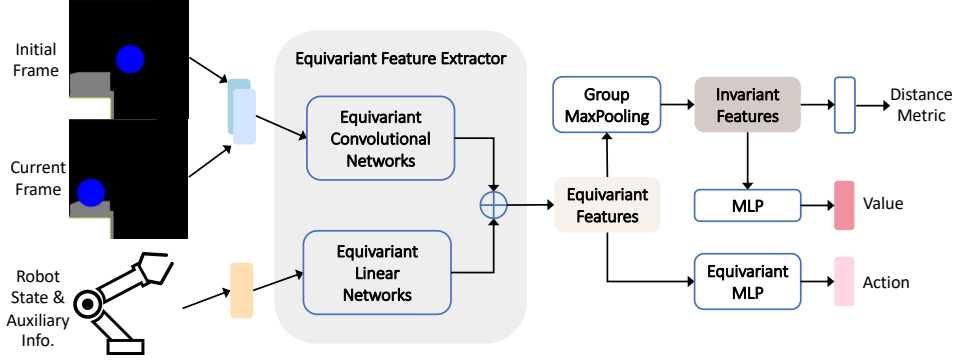


Figure 3: Equivariant policy network architecture.

147 **Equivariant feature extractor.** In real manipulation tasks, the observations typically comprise
 148 multiple modalities, such as image observations, robot proprioceptive states, and goal positions
 149 represented in vector form. To accommodate these diverse modalities, we designed an equivariant
 150 feature extractor h^{equi} , that employs an equivariant convolutional network h^{eConv} [36] for image
 151 processing, coupled with an equivariant linear network h^{eMLP} [38] to handle vector inputs. The
 152 resulting equivariant features from these two pathways are concatenated to form the output of the
 153 feature extractor. Formally, $h^{equi}(s) = \text{Concat}(h^{eConv}(s), h^{eMLP}(s))$.

154 **Invariant value and equivariant policy.** In the context of MDPs involving robotic manipulation
 155 tasks with group symmetries, it is known that the optimal value function maintains group invari-
 156 ance, while the optimal policy displays group equivariance [28]. To attain this, both the policy and
 157 value networks utilize a shared equivariant feature extractor, designed to distill equivariant features
 158 from observations. Subsequently, the value network leverages a group pooling layer to transform
 159 these equivariant features into invariant ones, before employing a fully connected layer to generate
 160 values. Formally, $h^{inv}(s) = \text{GroupMaxPooling}(h^{equi}(s))$. The policy network, on the other hand,
 161 processes the equivariant features with an additional equivariant MLP network to output actions.

162 4.4 Unsupervised Dynamic Policy Assignment

163 In COVERS, we propose to detect different groups of tasks
 164 based on *distances in the invariant feature space*. Such a
 165 mechanism facilitates knowledge transfer between tasks in
 166 each group. At a fixed episode interval, COVERS selects the
 167 policy of the group, whose data buffer \mathcal{B} has the minimal dis-
 168 tance in the invariant feature space to the rollout buffer \mathcal{O} col-
 169 lected in the current environment. Note that the invariant fea-
 170 tures of both \mathcal{O} and \mathcal{B} are obtained through the feature extrac-
 171 tor of π as shown in Figure 4. Considering that \mathcal{O} and \mathcal{B} may
 172 have a different number of data pairs, we take a probabilistic
 173 perspective by treating those data buffers as sample-based rep-
 174 resentations of two distributions and use the Wasserstein distance to measure the distance between
 175 those two feature distributions. The invariant features are obtained from the equivariant feature
 176 extractor via a group max-pooling operation as shown in Figure 3.

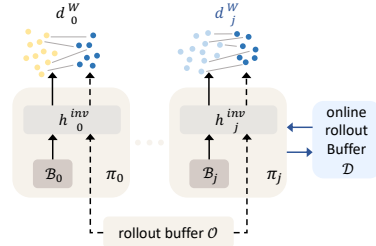


Figure 4: Calculation of 1-Wasserstein distance and update of selected policy π_j , whose data buffer has minimal distance to \mathcal{O} .

177 **Wasserstein distance on invariant feature space.** Let \mathbf{X} and \mathbf{Y} be a matrix constructed by invari-
 178 ant features extracted from the state buffer \mathcal{B} of size n and the buffer \mathcal{O} of size m . Concretely,
 179 $\mathbf{X} = (X_1, X_2, \dots, X_n)^T$, $X_i = h^{inv}(s_i)$, $i \in [n]$, $s_i \in \mathcal{B}$, and $\mathbf{Y} = (Y_1, Y_2, \dots, Y_m)^T$, $Y_l =$
 180 $h^{inv}(s_l)$, $l \in [m]$, $s_l \in \mathcal{O}$. We use the 1-Wasserstein distance [39] to measure the distance between
 181 two empirical distributions \mathbf{X} and \mathbf{Y} . Hence the distance between \mathcal{O} and \mathcal{B} is

$$d^W(\mathcal{O}, \mathcal{B}) = W_1(\mathbf{X}, \mathbf{Y}) = \min_{\gamma} \langle \gamma, \mathbf{M} \rangle_F \text{ s.t. } \gamma \mathbf{1} = \mathbf{a}, \gamma^T \mathbf{1} = \mathbf{b}, \gamma \geq 0, \quad (2)$$

182 where $\mathbf{M}_{i,l} = \|X_i - Y_l\|_2$, $\mathbf{a} = [1/n, \dots, 1/n]$, $\mathbf{b} = [1/m, \dots, 1/m]$. \mathbf{M} is the metric cost matrix.

183 **5 Simulation Experiments**

184 We validate COVERS’s performance in robot manipulation [40] tasks with nonstationary environ-
 185 ments containing different objects or following different reward functions. We aim to investigate
 186 whether our method can (1) recall stored policy when facing a seen group, as well as automatically
 187 initialize a new policy when encountering an unseen group, (2) achieve similar or better performance
 188 compared to baselines, and (3) understand the significance of key components of COVERS.

189 **5.1 Environment**

190 **Simulation setup.** Our manipulation setup is composed of
 191 four groups of tasks. Each group contains four tasks, and all
 192 tasks within the same group exhibit rotational or reflectional
 193 symmetry with respect to each other. We build environments
 194 based on the Meta-World benchmark [40]. Meta-World fea-
 195 tures a variety of table-top manipulation tasks that require in-
 196 teraction with diverse objects using a Sawyer robot. We show
 197 the four groups of tasks in Figure 2 including **Goal Reach** for
 198 reaching a goal position, **Button Press** for pressing the button
 199 with gripper, **Drawer Close** for closing drawer with gripper,
 200 and **Plate Slide** for sliding the plate to a goal position. The
 201 goal positions and object locations of tasks in each group are
 202 symmetrically arranged around the center of the table.

203 **States and actions.** The agent receives four kinds of observa-
 204 tions: an RGB image captured by a top-down camera centered
 205 over the table at each timestep, an RGB image captured by the
 206 same camera at the beginning of the episode, the robot state in-
 207 cluding gripper’s 3D coordinates and opening angle, and aux-
 208 iliary information. The RGB image at the initial step helps al-
 209 leviate the occlusion problem caused by the movement of the
 210 robot. The auxiliary information contains 3D goal positions which are only revealed to the agent in
 211 Goal Reach since the goal locations are not visualized in the captured image, and are masked out for
 212 other groups. To close the sim-to-real gap, we preprocess the RGB images by inpainting robot arms
 213 motivated by [41], with details deferred to Section B.1. A comparison of the original and processed
 214 images is visualized in Figure 5. The action is a four-dimensional vector containing the gripper’s 3D
 215 positions and its opening angle. Considering that we utilize two distinct robots: Sawyer in the sim-
 216 ulation and Kinova in the real-world, such an action space and the image preprocessing mechanism
 217 help improve transferability between different robot morphologies.

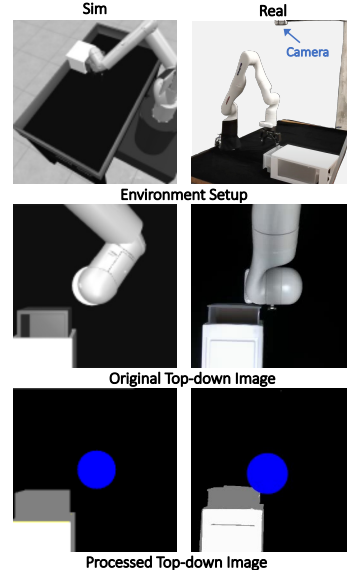


Figure 5: Image preprocessing to narrow down the sim-to-real gap.

218 **5.2 Baselines and Ablations**

219 We compare COVERS with different methods detailed as follows. **3RL** [22], an acronym for
 220 Replay-based Recurrent RL, is a state-of-the-art method in CRL with Meta-World tasks that in-
 221 tegrates experience replay [14] and recurrent neural networks [42]. Note that we augment **3RL** with
 222 a convolutional neural network (CNN) to handle image inputs. In contrast, **CLEAR** [14], a com-
 223 mon baseline of CRL, only utilize the experience replay by maintaining a memory buffer to store
 224 the experience of the past tasks and oversamples the current tasks to boost the performance in the
 225 current one. **Equi** utilizes a single policy with an equivariant feature extractor to solve all tasks.
 226 **CNN** utilizes a single policy with a CNN-based feature extractor as a vanilla baseline. We provide
 227 the detailed implementation of baselines and hyperparameters in Section B.

228 We compare with two ablation methods. **COVERS-GT** uses ground truth group labels to assign
 229 policies to different groups, which helps ablate the performance of our proposed policy assignment
 230 mechanism. **COVERS-CNN** utilizes a vanilla CNN block as the image feature extractor to help
 231 ablate the effect of using equivariant feature extractors.

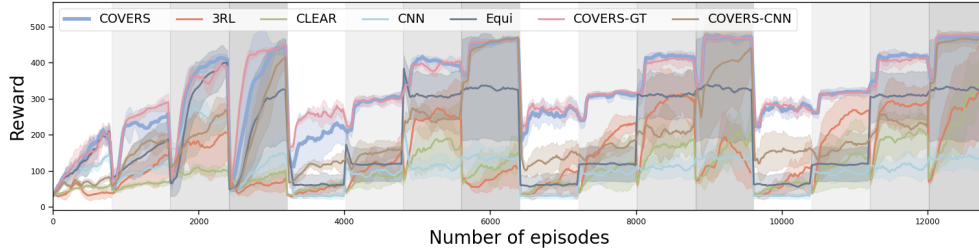


Figure 6: Training curves for COVERS and other methods. Each background color corresponds to one task group. COVERS shows similar performance with COVERS-GT, which utilizes additional ground truth group indices, and substantially outperforms other baselines.

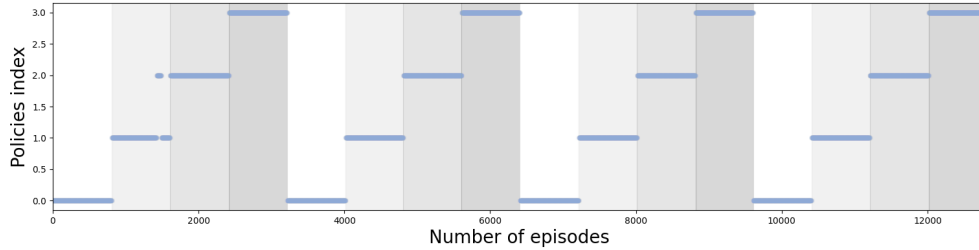


Figure 7: The selected policies at each episode of COVERS. Each background color corresponds to one task group. The assigned policy indexes remain in alignment with the ground truth ones.

232 6 Simulation Results and Ablations

233 6.1 Results

234 **Dynamic policy assignments.** Figure 7 shows that when the environment switches to a new group,
 235 COVERS quickly detects changes and initializes a new policy for the group. Our method also
 236 recalls the corresponding policy from the collection when facing the same group again. Overall, the
 237 dynamic policy assignments generated by COVERS align well with the ground truth group labels.
 238 However, we observe some instances where the policy assignment does not match the ground truth.
 239 This could potentially be attributed to the fact that the feature extractor of each policy may not be
 240 able to capture representative features for each group during the early stages of training. Notably,
 241 the rate of such misclassifications significantly reduces as the number of training episodes increases.

242 **Training performance.** We show the training curves of all methods in Figure 6 and the quantitative
 243 performance in Table 2, including the average success rates and mean rewards. COVERS achieves
 244 a much higher episode reward and success rate consistently in different groups than baselines. It is
 245 worth noting that although 3RL performs worse than COVERS, it achieves better performance than
 246 baselines with implicit task representations, including Equi, CLEAR, and CNN. This indicates that
 247 the explicit task representation used by 3RL, which maps transition pairs to latent variables using
 248 an RNN, facilitates the revelation of partial task identifications, thereby enhancing performance. It
 249 underscores the significance of task-specific representations in CRL.

250 In the early stages of training, there isn't a significant performance difference between COVERS
 251 and Equi. However, as training progresses, COVERS begins to outperform Equi. This is because
 252 COVERS avoids the problem of forgetting through the retraining of policies for each previously en-
 253 countered task group. A comparison between CNN and Equi reveals that incorporating group sym-
 254 metries as inductive bias within the equivariant network significantly enhances sample efficiency.
 255 This is achieved by only optimizing the policy for the abstracted MDP of each task group.

256 6.2 Ablation Study

257 **The effect of group symmetric information.** COVERS-CNN devoid of the invariant feature ex-
 258 tractor demonstrates lower episodic rewards and success rates when compared with COVERS as

Table 1: Quantitative results showing performances at convergence for different methods.

Methods		COVERS	3RL	CLEAR	CNN	Equi	COVERS-GT	COVERS-CNN
Plate Slide	Success Rate	0.97 ± 0.02	0.28 ± 0.06	0.06 ± 0.03	0.03 ± 0.02	0.02 ± 0.02	0.91 ± 0.03	0.62 ± 0.05
	Ave. Reward	344.04 ± 12.89	101.20 ± 7.35	65.65 ± 2.23	23.44 ± 1.14	64.02 ± 5.85	337.44 ± 13.87	232.25 ± 14.24
Button Press	Success Rate	0.87 ± 0.04	0.52 ± 0.06	0.31 ± 0.06	0.09 ± 0.03	0.01 ± 0.01	0.87 ± 0.04	0.26 ± 0.05
	Ave. Reward	323.41 ± 3.48	260.80 ± 6.86	138.78 ± 12.23	91.34 ± 9.34	121.13 ± 7.02	330.56 ± 2.63	181.21 ± 10.83
Drawer Close	Success Rate	0.82 ± 0.04	0.40 ± 0.06	0.27 ± 0.05	0.16 ± 0.04	0.40 ± 0.05	0.98 ± 0.02	0.56 ± 0.05
	Ave. Reward	400.09 ± 6.18	280.62 ± 6.39	216.08 ± 7.68	116.33 ± 10.1	273.26 ± 9.67	417.38 ± 5.6	227.3 ± 13.0
Goal Reach	Success Rate	0.98 ± 0.02	0.60 ± 0.06	0.58 ± 0.06	0.14 ± 0.04	0.47 ± 0.05	0.97 ± 0.02	0.97 ± 0.02
	Ave. Reward	483.53 ± 1.35	322.23 ± 17.33	293.5 ± 16.16	151.24 ± 14.31	306.72 ± 20.34	488.02 ± 0.35	480.96 ± 1.05
Average	Success Rate	0.91 ± 0.02	0.44 ± 0.03	0.30 ± 0.03	0.1 ± 0.02	0.22 ± 0.02	0.93 ± 0.01	0.60 ± 0.03
	Ave. Reward	387.77 ± 5.02	241.21 ± 7.39	178.5 ± 7.58	95.59 ± 5.59	191.28 ± 8.23	393.35 ± 5.19	280.43 ± 8.49

shown in Table 1 and Figure 6. From these results, we conclude that the equivariant feature extractor significantly enhances performance by modeling group symmetry information by introducing beneficial inductive bias through its model architecture.

The effect of the dynamic policy assignment module In Figure 6, COVERs’s training curve is similar to COVERs-GT, which uses ground truth group indexes as extra prior knowledge. Table 1 shows that the performance drop due to misclassification is minor considering the small standard deviation and COVERs’s performance is within one or two standard deviations of COVERs-GT.

7 Real-world Validation

Real-world setup. Our real-world experiment setup utilizes a Kinova GEN3 robotic arm with a Robotiq 2F-85 gripper. The top-down RGB image is captured with an Intel RealSense D345f. Gripper’s coordinates and opening angle are obtained through the robot’s internal sensors. The real robot setups are demonstrated in Figure 8. We directly deploy the trained policies in simulation to the real world. Table 2 shows average success rates across 20 trials and shows that our trained policies have strong generalization capability to real-world scenarios. The performance drop compared with simulation experiments may be due to the inconsistent visual features and different scales of robots’ action spaces.

Task Groups	Success Rate
Plate Slide	0.45 ± 0.15
Button Press	0.60 ± 0.15
Drawer Close	0.65 ± 0.15
Goal Reach	0.95 ± 0.07

Table 2: Real-world validation results.

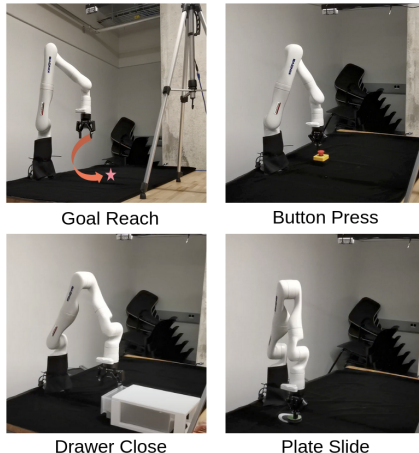


Figure 8: The real Kinova GEN3 setup with four task groups. The goal point marked in the figure is only disclosed to the agent in Goal Reach as auxiliary information.

8 Conclusion

We propose COVERs, a novel Vision-based CRL framework that leverages group symmetries to facilitate generalization to unseen but equivalent tasks under the same group operations. COVERs detects group boundaries in an unsupervised manner based on invariant features and grows policies for each group of equivalent tasks instead of a single task. We show that COVERs assigns tasks to different groups with high accuracy and has a strong generalization capability, outperforming baselines by a large margin. One limitation of COVERs is that the memory it occupies grows linearly with the number of task groups. However, it is worth noting that COVERs still occupies less memory than maintaining a policy buffer for each task by only storing representative data frames such as the initial frames for each task group. Another limitation is that although assuming a top-down camera with a fixed base is widely adopted in existing works, it is hard to fulfill outside of labs. It would be interesting to incorporate more general group operations, such as affine transformation and domain randomization techniques, to handle deformed images. Another interesting future direction is extending our work to continual multi-agent RL settings.

References

- [1] C. Finn, P. Abbeel, and S. Levine. Model-agnostic meta-learning for fast adaptation of deep networks. In *International Conference on Machine Learning*, pages 1126–1135. PMLR, 2017.
- [2] A. Nagabandi, C. Finn, and S. Levine. Deep online learning via meta-learning: Continual adaptation for model-based rl. *arXiv preprint arXiv:1812.07671*, 2018.
- [3] A. Nagabandi, I. Clavera, S. Liu, R. S. Fearing, P. Abbeel, S. Levine, and C. Finn. Learning to adapt in dynamic, real-world environments through meta-reinforcement learning. *arXiv preprint arXiv:1803.11347*, 2018.
- [4] W. Zhao, J. P. Queralta, and T. Westerlund. Sim-to-real transfer in deep reinforcement learning for robotics: a survey. In *2020 IEEE Symposium Series on Computational Intelligence (SSCI)*, pages 737–744. IEEE, 2020.
- [5] K. Kheterpal, M. Riemer, I. Rish, and D. Precup. Towards continual reinforcement learning: A review and perspectives. *Journal of Artificial Intelligence Research*, 75:1401–1476, 2022.
- [6] K. Kheterpal, M. Riemer, I. Rish, and D. Precup. Towards continual reinforcement learning: A review and perspectives. *arXiv preprint arXiv:2012.13490*, 2020.
- [7] M. Xu, W. Ding, J. Zhu, Z. Liu, B. Chen, and D. Zhao. Task-agnostic online reinforcement learning with an infinite mixture of gaussian processes. *Advances in Neural Information Processing Systems*, 33:6429–6440, 2020.
- [8] H. Ren, A. Sootla, T. Jafferjee, J. Shen, J. Wang, and H. Bou-Ammar. Reinforcement learning in presence of discrete markovian context evolution. *arXiv preprint arXiv:2202.06557*, 2022.
- [9] A. Xie, J. Harrison, and C. Finn. Deep reinforcement learning amidst continual structured non-stationarity. In *International Conference on Machine Learning*, pages 11393–11403. PMLR, 2021.
- [10] J. Schulman, F. Wolski, P. Dhariwal, A. Radford, and O. Klimov. Proximal policy optimization algorithms. *arXiv preprint arXiv:1707.06347*, 2017.
- [11] S. Thrun and T. M. Mitchell. Lifelong robot learning. *Robotics and autonomous systems*, 15(1-2):25–46, 1995.
- [12] F. Tanaka and M. Yamamura. An approach to lifelong reinforcement learning through multiple environments. In *6th European Workshop on Learning Robots*, pages 93–99, 1997.
- [13] Z. Chen and B. Liu. Lifelong machine learning. *Synthesis Lectures on Artificial Intelligence and Machine Learning*, 12(3):1–207, 2018.
- [14] D. Rolnick, A. Ahuja, J. Schwarz, T. Lillicrap, and G. Wayne. Experience replay for continual learning. *Advances in Neural Information Processing Systems*, 32, 2019.
- [15] M. Xu, Z. Liu, P. Huang, W. Ding, Z. Cen, B. Li, and D. Zhao. Trustworthy reinforcement learning against intrinsic vulnerabilities: Robustness, safety, and generalizability. *arXiv preprint arXiv:2209.08025*, 2022.
- [16] J. Kirkpatrick, R. Pascanu, N. Rabinowitz, J. Veness, G. Desjardins, A. A. Rusu, K. Milan, J. Quan, T. Ramalho, A. Grabska-Barwinska, et al. Overcoming catastrophic forgetting in neural networks. *Proceedings of the national academy of sciences*, 114(13):3521–3526, 2017.
- [17] S. Powers, E. Xing, E. Kolve, R. Mottaghi, and A. Gupta. Cora: Benchmarks, baselines, and metrics as a platform for continual reinforcement learning agents. In *Conference on Lifelong Learning Agents*, pages 705–743. PMLR, 2022.

- 324 [18] H. Ahn, S. Cha, D. Lee, and T. Moon. Uncertainty-based continual learning with adaptive
325 regularization. *Advances in neural information processing systems*, 32, 2019.
- 326 [19] R. Traoré, H. Caselles-Dupré, T. Lesort, T. Sun, G. Cai, N. Díaz-Rodríguez, and D. Fil-
327 liat. Discorl: Continual reinforcement learning via policy distillation. *arXiv preprint*
328 *arXiv:1907.05855*, 2019.
- 329 [20] S. Sæmundsson, K. Hofmann, and M. P. Deisenroth. Meta reinforcement learning with latent
330 variable gaussian processes. *arXiv preprint arXiv:1803.07551*, 2018.
- 331 [21] W. Yu, J. Tan, C. K. Liu, and G. Turk. Preparing for the unknown: Learning a universal policy
332 with online system identification. *arXiv preprint arXiv:1702.02453*, 2017.
- 333 [22] M. Caccia, J. Mueller, T. Kim, L. Charlin, and R. Fakoore. Task-agnostic continual reinforce-
334 ment learning: In praise of a simple baseline. *arXiv preprint arXiv:2205.14495*, 2022.
- 335 [23] A. Chaudhry, M. Rohrbach, M. Elhoseiny, T. Ajanthan, P. K. Dokania, P. H. Torr, and M. Ran-
336 zato. Continual learning with tiny episodic memories. 2019.
- 337 [24] B. Ravindran and A. G. Barto. Symmetries and model minimization in markov decision pro-
338 cesses, 2001.
- 339 [25] B. Ravindran and A. G. Barto. Approximate homomorphisms: A framework for non-exact
340 minimization in markov decision processes. 2004.
- 341 [26] E. van der Pol, D. Worrall, H. van Hoof, F. Oliehoek, and M. Welling. Mdp homomorphic
342 networks: Group symmetries in reinforcement learning. *Advances in Neural Information Pro-*
343 *cessing Systems*, 33:4199–4210, 2020.
- 344 [27] E. van der Pol, H. van Hoof, F. A. Oliehoek, and M. Welling. Multi-agent mdp homomorphic
345 networks. *arXiv preprint arXiv:2110.04495*, 2021.
- 346 [28] D. Wang, R. Walters, and R. Platt. So (2) equivariant reinforcement learning. In *International*
347 *conference on learning representations (ICLR)*, 2022.
- 348 [29] D. Wang, R. Walters, X. Zhu, and R. Platt. Equivariant q learning in spatial action spaces. In
349 *Conference on Robot Learning*, pages 1713–1723. PMLR, 2022.
- 350 [30] L. Zhao, X. Zhu, L. Kong, R. Walters, and L. L. Wong. Integrating symmetry into differentiable
351 planning with steerable convolutions. In *The Eleventh International Conference on Learning*
352 *Representations*, 2023.
- 353 [31] D. Wang, J. Y. Park, N. Sortur, L. L. Wong, R. Walters, and R. Platt. The surprising effective-
354 ness of equivariant models in domains with latent symmetry. *arXiv preprint arXiv:2211.09231*,
355 2022.
- 356 [32] X. Zhu, D. Wang, O. Biza, G. Su, R. Walters, and R. Platt. Sample efficient grasp learning
357 using equivariant models. *arXiv preprint arXiv:2202.09468*, 2022.
- 358 [33] T. Cohen and M. Welling. Group equivariant convolutional networks. In *International confer-*
359 *ence on machine learning*, pages 2990–2999. PMLR, 2016.
- 360 [34] F. Fuchs, D. Worrall, V. Fischer, and M. Welling. Se (3)-transformers: 3d roto-translation
361 equivariant attention networks. *Advances in Neural Information Processing Systems*, 33:1970–
362 1981, 2020.
- 363 [35] M. J. Hutchinson, C. Le Lan, S. Zaidi, E. Dupont, Y. W. Teh, and H. Kim. Lietransformer:
364 Equivariant self-attention for lie groups. In *International Conference on Machine Learning*,
365 pages 4533–4543. PMLR, 2021.

- 366 [36] M. Weiler and G. Cesa. General $e(2)$ -equivariant steerable cnns. *Advances in Neural Information Processing Systems*, 32, 2019.
367
- 368 [37] M. Finzi, M. Welling, and A. G. Wilson. A practical method for constructing equivariant
369 multilayer perceptrons for arbitrary matrix groups. In *International Conference on Machine*
370 *Learning*, pages 3318–3328. PMLR, 2021.
- 371 [38] G. Cesa, L. Lang, and M. Weiler. A program to build $e(n)$ -equivariant steerable CNNs. In
372 *International Conference on Learning Representations*, 2022. URL [https://openreview.](https://openreview.net/forum?id=WE4qe9xlnQw)
373 [net/forum?id=WE4qe9xlnQw](https://openreview.net/forum?id=WE4qe9xlnQw).
- 374 [39] V. I. Bogachev and A. V. Kolesnikov. The monge-kantorovich problem: achievements, con-
375 nections, and perspectives. *Russian Mathematical Surveys*, 67(5):785, 2012.
- 376 [40] T. Yu, D. Quillen, Z. He, R. Julian, K. Hausman, C. Finn, and S. Levine. Meta-world: A
377 benchmark and evaluation for multi-task and meta reinforcement learning. In *Conference on*
378 *Robot Learning*, pages 1094–1100. PMLR, 2020.
- 379 [41] S. Bahl, A. Gupta, and D. Pathak. Human-to-robot imitation in the wild. *arXiv preprint*
380 *arXiv:2207.09450*, 2022.
- 381 [42] B. Bakker. Reinforcement learning with long short-term memory. *Advances in neural infor-*
382 *mation processing systems*, 14, 2001.
- 383 [43] P. I. Etingof, O. Golberg, S. Hensel, T. Liu, A. Schwendner, D. Vaintrob, and E. Yudovina.
384 *Introduction to representation theory*, volume 59. American Mathematical Soc., 2011.

385 **A Brief Introduction to Group and Representation Theory**

386 In this section, we briefly introduce Group and Representation Theory [43] to help understand the
387 policy structure in Section B.2.

388 Linear group representations describe abstract groups in terms of linear transformations on some
389 vector spaces. In particular, they can be used to represent group elements as linear transformations
390 (matrices) on that space. A representation of a group G on a vector space V is a group homomor-
391 phism from G to $GL(V)$, the general linear group on V . That is, a representation is a map

$$\rho: G \rightarrow GL(V), \quad \text{such that} \quad \rho(g_1 g_2) = \rho(g_1) \rho(g_2), \quad \forall g_1, g_2 \in G. \quad (3)$$

392 Here V is the representation space, and the dimension of V is the dimension of the representation.

393 **A.1 Trivial Representation**

394 Trivial representation maps any group element to the identity, i.e.

$$\forall g \in G, \rho(g) = 1. \quad (4)$$

395 **A.2 Irreducible Representations**

396 A representation of a group G is said to be irreducible (shorthand as **irrep**) if it has no non-trivial
397 invariant subspaces. For example, given a group G acting on a vector space V , V is said to be
398 irreducible if the only subspaces of V preserved under the action of every group element are the zero
399 subspace and V itself. The trivial representation is an irreducible representation and is common to
400 all groups.

401 **A.3 Regular Representation**

402 Given a group G , the regular representation is a representation over a vector space V which has a
403 basis indexed by the elements of G . In other words, if G has n elements (if G is finite), then the
404 regular representation is a representation on a vector space of dimension n . An important fact about
405 the regular representation is that it can be decomposed into irreducible representations in a very
406 structured way.

407 **A.4 Dihedral Group**

408 The dihedral group D_n is the group of symmetries of a regular n -sided polygon, including n rotations
409 and n reflections. Thus, D_n has $2n$ elements. For example, the dihedral group of a square (D_4)
410 includes 4 rotations and 4 reflections, giving 8 transformations in total.

411 **B Additional Experiment Details**

412 **B.1 Image Inpainting**

413 To close the sim-to-real gap, we employ a pre-processing technique on camera images, which in-
414 volves in-painting robotic arms. The process begins by capturing a background image in which
415 the robotic arm is absent from the camera’s view. For every time step, a mask that represents the
416 position of each robotic limb is generated, leveraging the 3D locations of individual joints and the
417 projection matrix of the camera. With this mask, we can select all areas devoid of the robotic arm,
418 and subsequently update the background image accordingly. The images are subjected to a color
419 correction process to mitigate any potential color deviations attributable to lighting or reflection.
420 Lastly, a distinct blue circle is overlaid at the gripper’s position on the background image to indicate
421 the gripper’s location. The entire image in-painting process is shown in Figure 9.

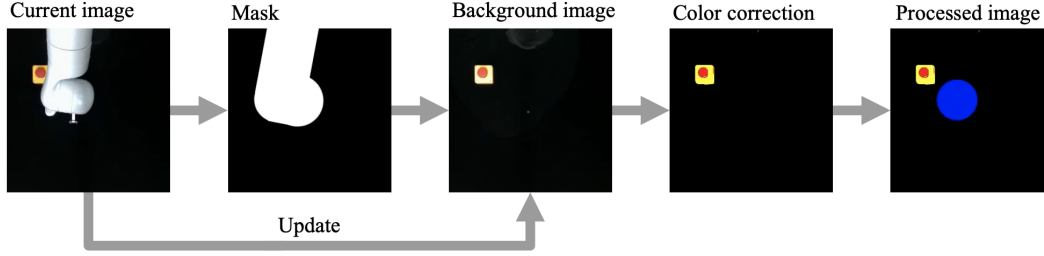


Figure 9: Image inpainting process.

422 B.2 Detailed Policy Architecture

423 In this section, we present the detailed model architecture including the model sizes and the types of
 424 each layer in Figure 10.

425 In order to make our policy network equivariant under transformations from the finite group D_2 ,
 426 we need to choose the appropriate representation for both the network input and output, while also
 427 ensuring that the network architecture and operations preserve this equivariance.

428 The image input is encoded using the trivial representation. The robot state, on the other hand, is
 429 encoded with a mixture of different representations: the gripper’s position on the z-axis and the
 430 gripper’s open angle are encoded with the trivial representation since they are invariant to group
 431 actions in D_2 . The gripper’s location on the x and y-axes, however, are encoded with two different
 432 non-trivial irreducible representations because their values are equivariant to group actions in D_2 .

433 The value output is encoded with the trivial representation since the optimal value function should
 434 be invariant to group actions [28]. Finally, the action output is encoded with a mixture of different
 435 representations. For actions, the gripper movement along the z-axis and the gripper’s opening angle
 436 are encoded with the trivial representation, while the gripper’s location on the x and y-axes are
 437 encoded with two different non-trivial irreducible representations, aligning with the input encoding.
 438 The distance metric is encoded with trivial representation through the group pooling operation.

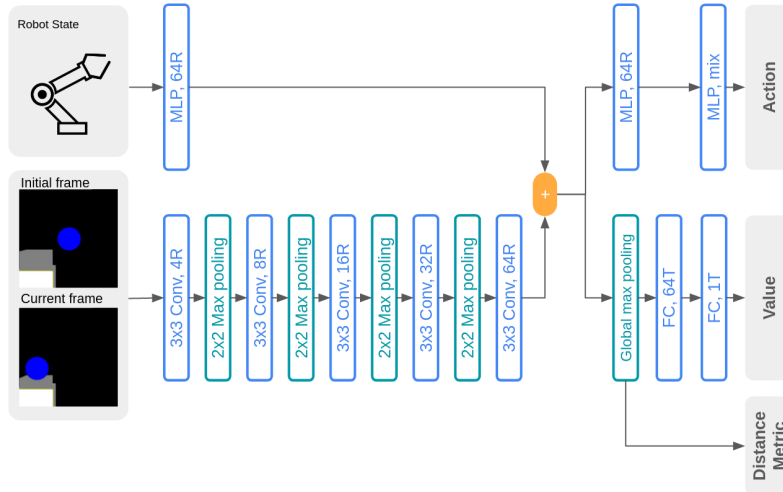


Figure 10: Detailed equivariant policy network architecture. ReLU nonlinearity is omitted in the figure. A layer with a suffix of R indicates the layer output is in the regular representation. A layer with a suffix of T indicates the layer output is in the trivial representation. A layer with a suffix of ‘mix’ means the layer output combines different representations.

439 **B.3 Implementation of CLEAR**

440 The CLEAR algorithm [14] addresses the challenge of continual learning by putting data from
 441 preceding tasks in a buffer, utilized subsequently for retraining. This method effectively decelerates
 442 the rate of forgetting by emulating a continuous learning setting. The specific network architecture
 443 for CLEAR is illustrated in Figure 11.

444 To make CLEAR able to process both images and robot state as input, we introduce a feature extrac-
 445 tor, which harmoniously integrates a CNN and an MLP network. This composite feature extractor
 446 is carefully designed to contain a similar quantity of learnable parameters to our Equivariant feature
 447 extractor.

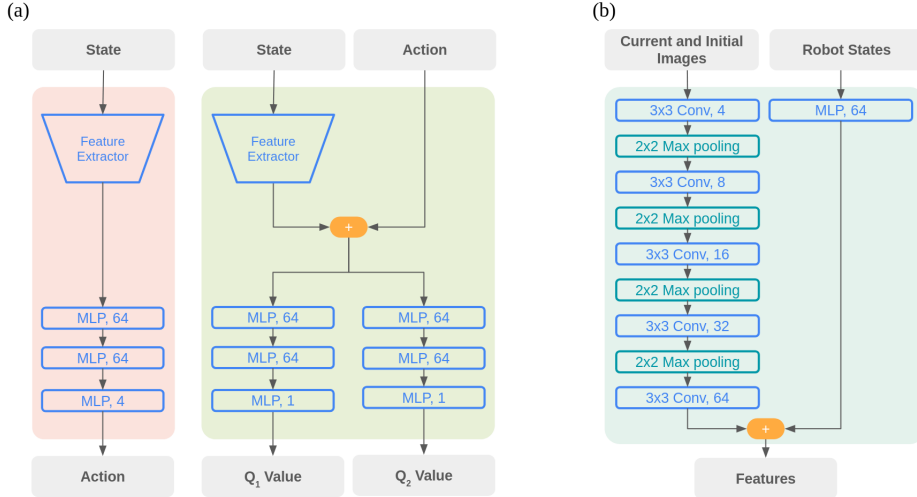


Figure 11: Network architecture for CLEAR. In (a) we show the network architecture of the actor network and the critic network. In (b) we show the structure of the feature extractor, which consists of both a CNN network and an MLP network. ReLU nonlinearity is omitted in the figure.

448 **B.4 Implementation of 3RL**

449 The 3RL algorithm [22] can be seen as an improved version of CLEAR, wherein additional historical
 450 data is provided to the actor and critic from a dedicated context encoder. This historical data includes
 451 (s_i, a_i, r_i) , and the context encoder extracted task specificities from the history data with an RNN
 452 network. The specific network architecture for 3RL is illustrated in Figure 12.

453 **B.5 Hyperparameters**

454 We show the hyperparameters of our proposed COVERS in Table 3. Moreover, we show the hyper-
 455 parameters of baselines in Table 4.

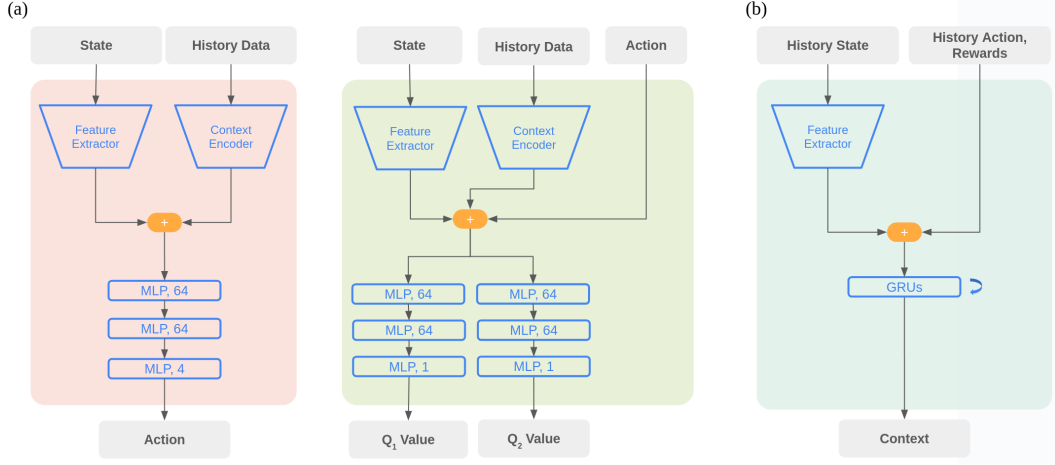


Figure 12: Network architecture for 3RL. In (a), we illustrate the structure of both the actor and critic networks, whereas (b) highlights the configuration of the context encoder, comprising a feature extractor and GRUs. It’s noteworthy that the feature extractor has the same architecture as the CLEAR algorithm, as shown in Figure 11.

Table 3: COVERS Hyperparameter

Hyperparameters	Value
Wasserstein distance threshold d_ϵ	1.0
Initial frame number k	4
Update interval N_u	1000
Rollout buffer size N_s	1000
Batch size	64
Number of epochs	8
Discount factor	0.99
Optimizer learning rate	0.0003
Likelihood ratio clip range ϵ	0.2
Advantage estimation λ	0.95
Entropy coefficient	0.001
Max KL divergence	0.05

Table 4: CLEAR and 3RL Hyperparameter

Hyperparameters	Value
Common hyperparameter	
Replay buffer size	200000
Discount factor	0.95
Burn in period	20000
Warm up period	1000
Batch size	512
Gradient clipping range	(-1.0, +1.0)
Learning rate	0.0003
Entropy regularization coefficient	0.005
3RL Specific Hyperparameters	
RNN’s number of layers	1
RNN’s context size	30
RNN’s context length	5